JACS
JOURNAL OF THE AMERICAN CHEMICAL SOCIETY
Article
pubs.acs.org/JACS

Dynamics of the Special Pair of Chlorophylls of Photosystem II

Daniele Narzi,[†] Daniele Bovi,[†] Pietro De Gaetano,[‡] and Leonardo Guidoni*[,†]

[†]University of L'Aquila, 67100 L'Aquila, Italy
[‡]La Sapienza - University of Rome, 00185 Roma, Italy

Supporting Information

ABSTRACT: Cholophylls are at the basis of the photosynthetic energy conversion mechanisms in algae, plants, and cyanobacteria. In photosystem II, the photoproduced electrons leave a special pair of chlorophylls (namely, P_{D1} and P_{D2}) that becomes cationic. This oxidizing pair $[P_{D1},P_{D2}]^+$, in turn, triggers a cascade of oxidative events, eventually leading to water splitting and oxygen evolution. In the present work, using quantum mechanics/molecular mechanics calculations, we investigate the electronic structure and the dynamics of the $P_{D1}P_{D2}$ special pair in both its oxidized and reduced states. In agreement with previously reported static calculations, the symmetry between the two chlorophylls was found to be broken, the positive charge being preferentially located on P_{D1}. Nevertheless, this study reveals for the first time that large charge fluctuations occur along dynamics, temporarily inverting the charge preference for the two branches. Finally, a vibrational analysis pinpointed that such charge fluctuations are strongly coupled to specific modes of the special pair.

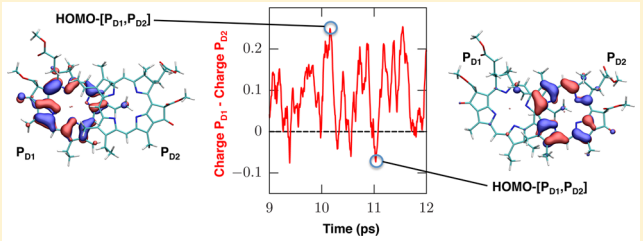

INTRODUCTION

When two and a half billion years ago the ancestors of cyanobacteria started to perform the photosynthetic water oxidation, molecular oxygen was released into the atmosphere leading to a deep transformation of the biosphere on the Earth. Since then, plants, algae, and cyanobacteria use photosystem II (PSII) in order to catalyze the water oxidation reaction, thus converting the light energy absorbed from the Sun into chemical energy.[1]

Photosystem II is a membrane protein complex, acting in the thylakoid membrane of oxygenic photosynthetic organisms as a water/plastoquinone oxidoreductase.[2] The light energy necessary to perform its catalytic function is first absorbed by the antenna system (i.e., a network of protein/pigment complexes) and afterward transferred to the reaction center (RC) of PSII.[3] Here, a charge separation occurs, leading to the oxidation of the substrate water molecules, taking place on the Mn_4CaO_5 oxygen evolving complex (OEC), and to O_2 release. Apart from the Mn_4CaO_5 cluster, the reaction center of PSII consists also of two polypeptide chains (D1 and D2), the chlorophyll *a* "special pair" (P_{D1} and P_{D2}), the two accessory chlorophylls *a* (Chl_{D1} and Chl_{D2}), two pheophytins *a* (Ph_{D1} and Ph_{D2}), two quinones (QA and QB), and a bicarbonate ion (BCT) coordinated with a non-heme iron (see Figure 1).

Intriguingly, the cofactors embedded in the reaction center are organized in a pseudo-C_2 symmetry, being arranged in two branches differing mainly by the presence or absence of the Mn_4CaO_5 cluster. Despite their geometric symmetry, the two branches show different activities. On the D1 side, where the OEC is located, after the charge separation occurring on the Chl_{D1},[4] an electron is removed from the neighboring tyrosine, Tyr-Z, which in turn oxidizes the Mn_4CaO_5 cluster, generating a sufficient oxidation power to oxidize the substrate water molecules. On the acceptor side, the electron is therefore transferred from Chl_{D1} to Phe_{D1}, which in turn reduces the final electron acceptor, the quinone, to hydroquinone, finally released into the thylakoid membrane.[5] In contrast, the D2 branch shows no primary electron transfer activity,[6,7] and it is thought to have a role in the protection of the reaction center of PSII from uncontrolled oxidative reactions[8−10] and from photoinhibition.[11]

Accordingly with the functional asymmetry of the two RC branches, the radical cation generated on the special pair P_{D1}/P_{D2} after its oxidation was found to be mainly localized on the P_{D1} chlorophyll.[12,13] In this regard, based on the high-resolution crystal structure of PSII solved in 2011,[2] Saito et al. determined by static quantum mechanics/molecular mechanics(QM/MM) calculations the ratio between the charge assigned to P_{D1} and that assigned to P_{D2} within the oxidized special pair $(P_{D1}/P_{D2})^{\bullet+}$ to be ∼80/20.[14] They additionally suggested that such delocalization is mainly due to the electrostatic asymmetry of several conserved D1/D2 residues.[14,15] Nevertheless, local protein motions could affect the cationic distribution among the pigments in the RC region resulting in different charge separation pathways. At cryogenic temperature, for instance, different charge separation pathways were suggested to exist, maybe playing a role also under physiological conditions.[16] Still, at low temperatures, the excitation can be easily trapped on the Chl_{D1} chlorophyll, thus promoting the subsequent cationic localization on the adjacent P_{D1}.[5] It was additionally proposed that, in the presence

Received: October 8, 2015
Published: November 20, 2015

DOI: 10.1021/jacs.5b10523
J. Am. Chem. Soc. 2016, 138, 257−264

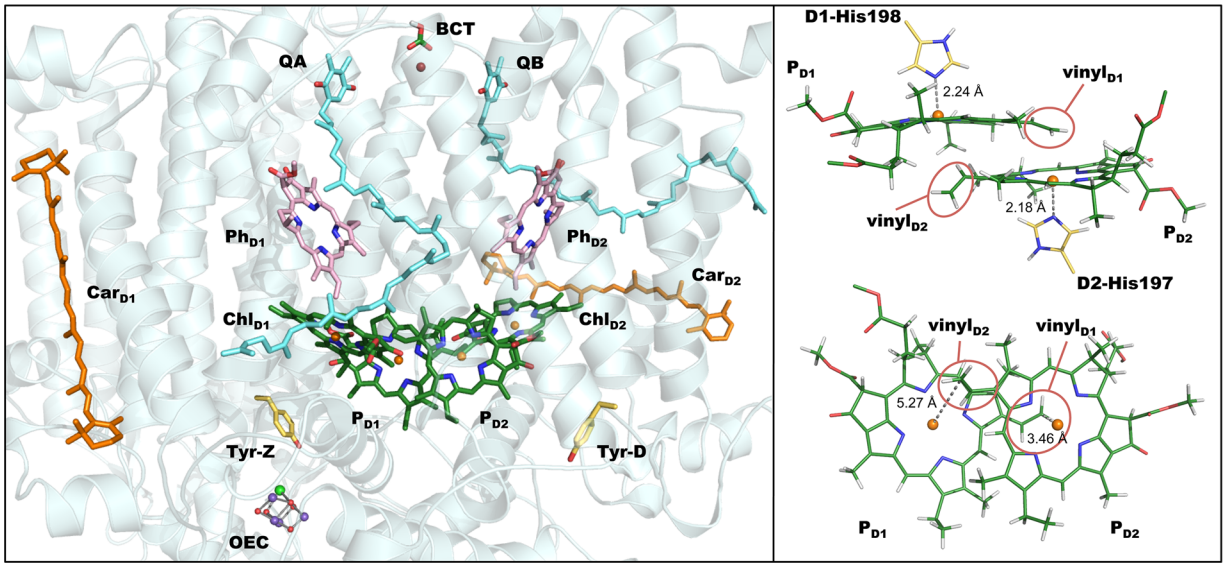

Figure 1. Simulated system. In the left panel, a portion of the simulated system is shown. The protein chains are represented as cartoons. The chlorophylls, β-carotene, pheophytins, plastoquinone, bicarbonate ion, and two tyrosines, Tyr-Z and Tyr-D, are shown in sticks. The Mn_4CaO_5 cluster is represented in balls and sticks. In the right panel, the region of the system treated at DFT level is shown in stick representation.

Table 1. Comparison of Charges[a]

	neutral system			oxidized system		
model	HOMO (% P_{D1})	LUMO (% P_{D1})	charge P_{D1}	HOMO-α (% P_{D1})	LUMO-β (% P_{D1})	charge P_{D1}
X-ray QM/MM	97.7	1.0	0.801			
Opt QM/MM	98.6	0.7	0.841	5.5	87.5	0.865
X-ray GP	58.6	5.6	0.549			
GP from Opt QM/MM	81.1	2.4	0.546	3.6	61.5	0.610
Opt GP	93.8	0.6	0.585	6.5	57.7	0.577
QM/MM MD	73.5 (29.9)	20.8 (30.4)	0.541 (0.05)	22.8 (23.9)	59.0 (6.5)	0.580 (0.060)

[a]Partial charge of P_{D1} calculated by static (X-ray and Opt) and dynamic (MD, averaged over the simulation time with standard deviations shown in brackets) calculations. The percent of HOMO and LUMO localized on P_{D1} is also shown. Calculations were performed in gas-phase (GP) and in QM/MM models, optimizing the systems in their respective oxidation state.

of high photon flux, the removal of the electron may result in a localization of the cation on the Chl_{D2} chlorophyll. In this case, the D2 branch could carry out a photoprotective function, promoting the electron transfer from the side-path donors (i.e., β-carotene (Car_{D2}), cytochrome *b*559, chlorophyll Z).[17,18]

In the last years, different structures of photosystem II at increasing resolution levels were solved by X-ray crystallography[2,19−22] shedding light on the atomistic details behind the catalytic function of PSII. Either way, it has to be pointed out that when the excitation reaches the reaction center of PSII, due to the thermal fluctuations, the excitation could be easily delocalized over the four central chlorophylls as well as the two pheophytins.[5] The subsequent localization of the cation on the P_{D1} chlorophyll occurs in the next tens of picoseconds.[12] An accurate investigation of the first steps of the oxidation of the special pair requires therefore a quantum mechanical description of the two P_{D1} and P_{D2} chlorophylls in their protein environment at physiological temperature.[4] The knowledge of the exact localization of the cation after the primary charge separation as well as the respective fluctuations turns out to be crucial to understand the catalytic function of PSII. In this respect, several studies were performed in the past decades, based on both experimental[12,13,23−26] and theoretical[4,14,15,27,28] approaches. Additionally, mixed experimental/theoretical studies turned out in recent years to shed light into the role of quantum coherence in determing the charge separation efficiency and clarify the influence of the vibrational modes on the electronic coherence.[29,30] Here, performing both static and molecular dynamics QM/MM calculations following a scheme already employed in recent works,[31,32] we characterized at physiological temperature the cationic state distribution over the $[P_{D1},P_{D2}]$ special pair in the reaction center of photosystem II. Our data reveals the crucial role of the dynamics in modulating the charge distribution, allowing us to identify the molecular motions that modulate the asymmetry of the two chlorophylls.

RESULTS

The distribution of the cationic state in the $[P_{D1},P_{D2}]$ special pair in the reaction center of PSII was first studied by means of DFT-based gas phase and QM/MM static calculations. In this context, the calculations were performed on the atomic positions determined by X-ray crystallography[2] as well as after geometry optimization of the quantum region.

In a second step, considering the same system and parameters used in the static QM/MM calculations, we carried out QM/MM molecular dynamics simulations, one in the electronic neutral state of the two chlorophylls, $[P_{D1},P_{D2}]^0_{AIMD}$, and the other in the oxidized state, $[P_{D1},P_{D2}]^{\bullet+}_{AIMD}$. The localization of the highest occupied molecular orbital as a

DOI: 10.1021/jacs.5b10523
J. Am. Chem. Soc. 2016, 138, 257−264

function of the time was determined for the neutral system, while in the oxidized system the dynamical localization of the electronic hole was monitored along the simulation time.

Static Calculations. Starting from the X-ray structure, after geometry optimization of the added hydrogens, we calculated in QM/MM framework the percent of HOMO and LUMO localized on the two P_{D1} and P_{D2} chlorophylls. We found that the HOMO is mainly localized on the P_{D1} chlorophyll (~97.7%) whereas the LUMO is more localized on the P_{D2} pigment (~99.0%). Consistent with these results, we also estimated the ratio between the charge localized on P_{D1} and that localized on P_{D2} after the removal of one electron from the quantum region. This ratio, hereafter indicated as $P_{D1}^{\bullet+}/P_{D2}^{\bullet+}$, was calculated to be 0.80/0.20 (see first line in Table 1). For clarity, it has to be pointed out that the charge localization determined on the neutral system was calculated after the removal of one electron from either the X-ray structure or the structures optimized in the neutral state in both the QM/MM and gas phase (GP) framework.

The X-ray structure was subsequently optimized considering the same QM/MM coupling scheme above employed (details reported in the Methods section) in both neutral and oxidized state. The calculation of the $P_{D1}^{\bullet+}/P_{D2}^{\bullet+}$ charge ratio showed a more localized cationic state on the P_{D1} chlorophyll after the optimization of the neutral system (second line in Table 1) with respect the structure determined by X-ray crystallography (0.84 vs 0.80). The localization is even stronger when the calculation is carried out on the structure optimized in the oxidized state (~0.87). These results are consistent with the respective localization of the HOMO and LUMO. Indeed, in the neutral state, the HOMO is well localized on the P_{D1} pigment indicating that the oxidation of the system will preferentially take place on this chlorophyll as in the case of the nonoptimized X-ray structure. Similarly, in the oxidized system, the LUMO is mainly localized on the P_{D1} chlorophyll, confirming that the electron hole is placed on it.

The calculations were repeated for the gas-phase model (GP) considering the atom positions found in the X-ray structure (X-ray GP in Table 1). Additionally, the calculations were repeated on the gas-phase models extracted from the two (neutral and oxidized) QM/MM optimized structures (GP from Opt QM/MM in Table 1) as well as on the two (neutral and oxidized) structures optimized in gas-phase (Opt GP in Table 1). As previously observed by Saito et al.,[14] the exclusion from the calculation of the electrostatic contribution due to the surrounding environment leads to a redistribution of the cationic charge over the two chlorophylls. Albeit the HOMO calculated on the neutral system remains more localized on the P_{D1} pigment, the $P_{D1}^{\bullet+}/P_{D2}^{\bullet+}$ charge ratio calculated after the removal of one electron decreases to ~0.55/0.45 in both the GP X-ray structure and the GP structure extracted from the optimized QM/MM system. The further optimization of the special pair in gas-phase (Opt GP in Table 1) leads to a $P_{D1}^{\bullet+}/P_{D2}^{\bullet+}$ charge ratio of ~0.59/0.41. Similar results were obtained for the GP models optimized in the oxidized state in the QM/MM framework (GP from Opt QM/MM in Table 1, $P_{D1}^{\bullet+}/P_{D2}^{\bullet+} \approx 0.61/0.39$) and in the gas-phase framework (Opt GP in Table 1, $P_{D1}^{\bullet+}/P_{D2}^{\bullet+} \approx 0.58/0.42$).

Our results confirm the importance of the electrostatic interactions between the special pair and the surrounding residues in determining the charge separation between the two pigments as already pointed out by previous studies.[14,15] Additionally, these results serve to validate the technical procedure adopted here in order to characterize the electronic structure and more specifically the cationic distribution over the chlorophyll special pair at finite temperature, as described in the next sections.

Dynamics of the Neutral Special Pair, $[P_{D1},P_{D2}]^0_{AIMD}$. Apart from the influence of the protein environment on the electronic properties of the special pair, the effects of the thermal fluctuations at physiological conditions could play an important role in the oxi-reduction properties of the P680. In order to investigate such aspect, we carried out QM/MM molecular dynamics simulations of the reaction center of photosystem II using the same level of theory employed in the static calculations. After ~3 ps of thermalization, the production run was carried out for ~12 ps, considering the system composed by the two P_{D1} and P_{D2} chlorophylls and the two respective coordinated histidines in their neutral state.

The average distribution of the HOMO over the two chlorophylls along the 12 ps of MD simulation showed a reduced localization on the P_{D1} pigment (73.5% see Table 1) with respect to the QM/MM calculation performed on the single X-ray structure (97.7%). Nevertheless, the time evolution of the HOMO distribution is characterized by large fluctuations (standard deviation ~30%) indicating the possibility of temporary inversions of such distribution over the two pigments. This behavior is clearly evident plotting the HOMO distribution over the time as reported in Figure 2.

Using structures extracted every 50 fs from the MD trajectory, we have additionally, performed single point calculations removing one electron from the system. In this way, we may estimate the partial charge present on the P_{D1} and the P_{D2} immediately after the oxidation and prior to structure

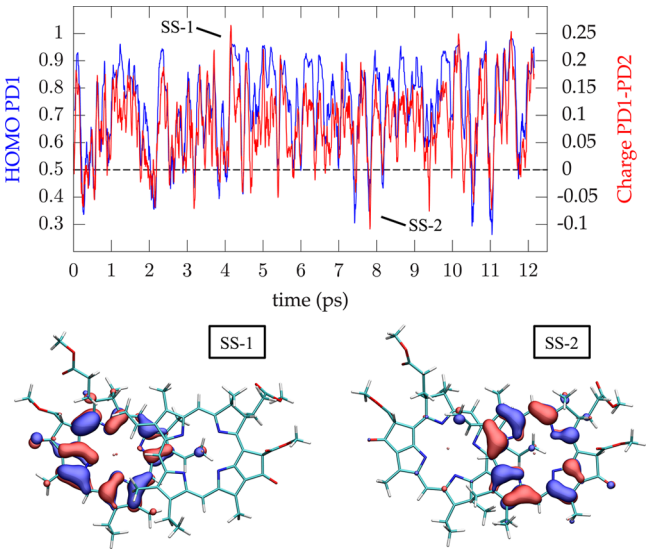

Figure 2. Neutral QM/MM simulation. In the top panel, the percent of HOMO localized on the P_{D1} chlorophyll is plotted as a function of the simualtion time (blue line). The difference of the partial charges present on the two chlorophylls calculated after the removal of one electron from the snapshots extracted by the neutral dynamics (red line) is also plotted. The value of the charge difference and the percent of HOMO are smoothed averaging over 10 frame blocks. In the bottom panel, the distribution of the HOMO over the two chlorophylls for two representative snapshots of the dynamics characterized by opposite charge distributions are shown as isosurface. Blue and red isosurfaces corresponds to electrons in the HOMO with, respectively, α and β spin momenta.

DOI: 10.1021/jacs.5b10523
J. Am. Chem. Soc. 2016, 138, 257−264

relaxation. The difference between the two charges as a function of the simulated time was reported in Figure 2 together with the time evolution of the HOMO distribution. As expected, the two plotted variables are highly correlated, and for values of the HOMO distribution smaller than 50%, the difference of the partial charges assumes negative values (i.e., the cationic charge is more localized on the P_{D2} chlorophyll). The average value of the charge ratio $P^{\bullet+}_{D1}/P^{\bullet+}_{D2}$ along the dynamic, reported in Table 1, was found to be equal to 0.54/0.46, appreciably smaller than the respective ratio calculated on the atomic positions in the X-ray structure. The HOMO for two representative snapshots corresponding to the maximum and minimum values of the charge ratio $P^{\bullet+}_{D1}/P^{\bullet+}_{D2}$ was also plotted with surface representation (see Figure 2) on the two structures, showing clearly the net distribution of this orbital on one of the two pigments. It has to be pointed out that the values reported in Figure 2 are smoothed for clarity. The original values of the partial charges P_{D1} and the P_{D2} pigments, as obtained from the QM/MM MD simulations and plotted in Figure 1S in Supporting Information, lead to a maximum $P^{\bullet+}_{D1}/P^{\bullet+}_{D2}$ value ≈ 0.7/0.3.

Dynamics of Oxidized Special Pair $[P_{D1},P_{D2}]^{\bullet+}_{AIMD}$. The first events occurring after the oxidation of the special pair were monitored by carrying out a QM/MM MD simulation after the removal of one electron from the QM system. A snapshot extracted from the neutral system trajectory, $[P_{D1},P_{D2}]^{0}_{AIMD}$, was taken as starting point of such simulation. In Figure 3, we report the time evolution of the LUMO distribution over P_{D1} along 8 ps of production run. Additionally, the partial charges present on the P_{D1} and the P_{D2} pigments were also computed, and their difference is reported in the same graphic. As expected, the LUMO was found to be mainly localized on the P_{D1} chlorophyll (on average ∼60% of the time, see also Table 1). Consistently, the partial (positive) charge localized on P_{D1} is ∼0.59 (see Table 1) and the difference between the partial charges distributed over the two pigments evolves in time following nearly the same trend of the LUMO distribution.

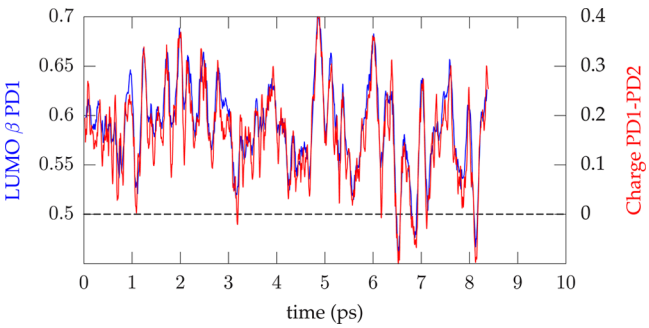

Figure 3. Charge fluctuations in the oxidized system. The percent of LUMO localized on the P_{D1} chlorophyll is plotted as a function of the simualtion time (blue line). The difference of the partial charges present on the two chlorophylls is also reported (red line). The value of the charge difference and the percent of LUMO are smoothed averaging over 10 frame blocks. Since the simulation of the neutral system was carried out removing an electron with spin α, the reported LUMO refers to the electron with the β spin.

The variance of the cationic distribution over the two chlorophylls due to the thermal fluctuations translate into episodic inversions of the cationic character of the pigments. In particular, the $P^{\bullet+}_{D1}/P^{\bullet+}_{D2}$ charge ratio was found to oscillate between a maximum value of ∼0.8/0.2 and a minimum value of ∼0.4/0.6 (see also Figure 2S in Supporting Information). These results clearly show that, apart from the electrostatic coupling of the $[P_{D1},P_{D2}]$ moiety with the protein environment, the thermal fluctuations play a crucial role modulating the cationic distribution over the two chlorophylls, at least in the first picoseconds following the oxidation event.

Charge Dynamics and Molecular Motion. The characteristic frequencies of the charge fluctuations of the oxidized special pair were obtained by Fourier analysis of the charge difference between P_{D1} and P_{D2}, as reported in the top panel of Figure 4. The picture indicates that the molecular motions influence the charge distribution on a broad range of frequencies. In order to understand which molecular vibrations are coupled to the characteristic frequencies of the charge fluctuations, we have also carried out the effective normal mode vibrational analysis of the $[P_{D1},P_{D2}]^{\bullet+}_{AIMD}$ trajectory (see Methods section). This procedure consists of decomposing the total vibrational density of states of the system into molecular motions, which are localized in frequency and represent the finite temperature analogues of the normal-mode analysis.

In the same plot, we also report the power spectra of four specific effective normal modes that have frequencies clearly resonating with the charge fluctuations on P_{D1} and P_{D2} chlorophylls. These modes are representative of bands that are involved in the charge modulations. More in detail, the low-frequency band (340−400 cm^{-1}) involves out of plane motions of the P_{D2} chlorophyll rings and magnesium−nitrogen stretching (e.g., P_{D2}−ENM C), whereas the high-frequency band in the range 1520−1600 cm^{-1} involves mainly the C−C and C−N stretching of the pyrrolic rings (rings I, II, and III) of the P_{D2} chlorophyll (e.g., P_{D2}−ENM B). In the middle range, between 650 and 800 cm^{-1}, we found several motions characteristic of the P_{D1} chlorophyll resonant with the charge fluctuation frequencies involving torsions of the pyrrolic rings I, II, and III and a band at 870 cm^{-1} resonant with motions involving the torsion of ring IV of P_{D1} and the Mg−N stretching (e.g., P_{D1}−ENM A). Additionally, the out of plane motions of ring III and the bending of the monomethyl ester of P_{D2} chlorophyll (P_{D2}−ENM D) seems to modulate the charge fluctuations at 790 cm^{-1}.

All the above-mentioned bands modulate the charge fluctuations by favoring or disfavoring charge localization on P_{D1} or P_{D2} via molecular distortions and coupling with the field of the environment. Considering the different environment surrounding the two pigments, we can suggest that motions of ring III of P_{D2} can be influenced by the proximity of the D2-Trp191. The same residue was suggested to be involved in the "saddling mode" of P_{D2} using s normal-coordinate structural decomposition.[15]

A number of modes that mostly contribute to selected characteristic frequencies of the charge fluctuations are identified and projected on the atoms of the P_{D1} and P_{D2} chlorophylls. With the purpose of defining which moiety of the two pigments most contributes to the modes extracted by the vibrational analysis, we reported the structure of the special pair in the bottom panel of Figure 4 with the atoms colored on the basis of the respective contribution to the previously identified modes.

Although there is an overall symmetry of the regions most contributing to such charge fluctuations, some specific differences are present between P_{D1} and P_{D2}. In particular, the Mg atom and the vinyl group bound to ring I are

DOI: 10.1021/jacs.5b10523
J. Am. Chem. Soc. 2016, 138, 257−264

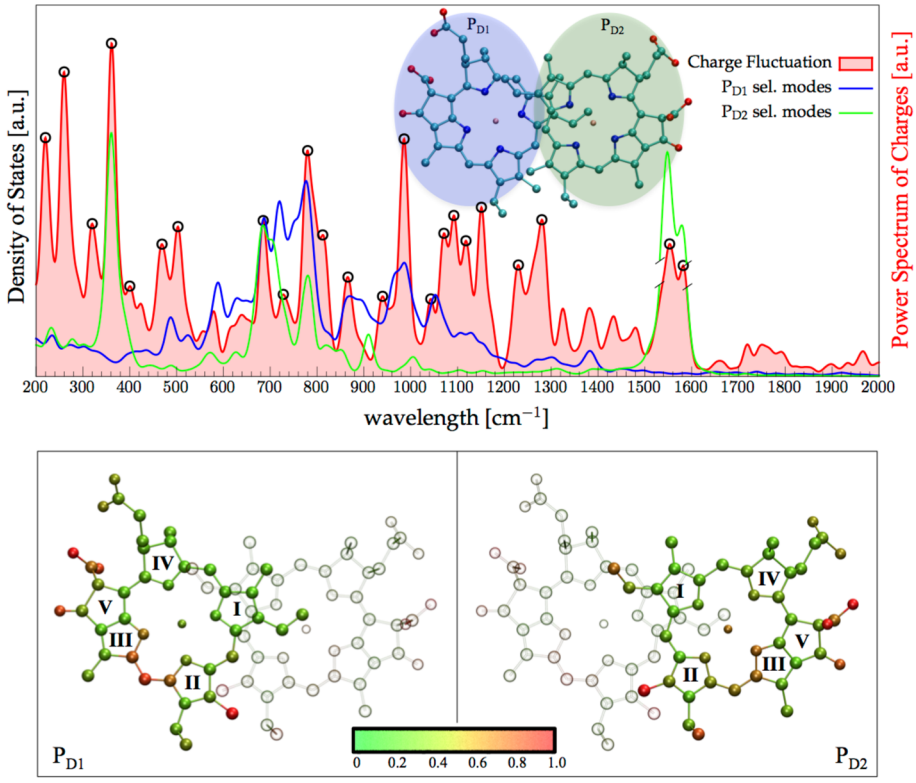

Figure 4. Charge fluctuation frequencies. (top) Frequencies of the charge fluctuations obtained by Fourier analysis on the QM/MM MD simulation of the oxidized system $[P_{D1},P_{D2}]^{\bullet+}_{AIMD}$ are shown in red. A set of four effective normal modes (ENM) representative of the motions of the P_{D1} and P_{D2} chlorophylls resonant with charge fluctuations are also reported. The ENMs are shown as solid lines for P_{D2} and dashed line for P_{D1}. (bottom) Structure of the special pair, coloring atoms based on the respective contribution to the ENMs resonant with the charge fluctuation frequencies.

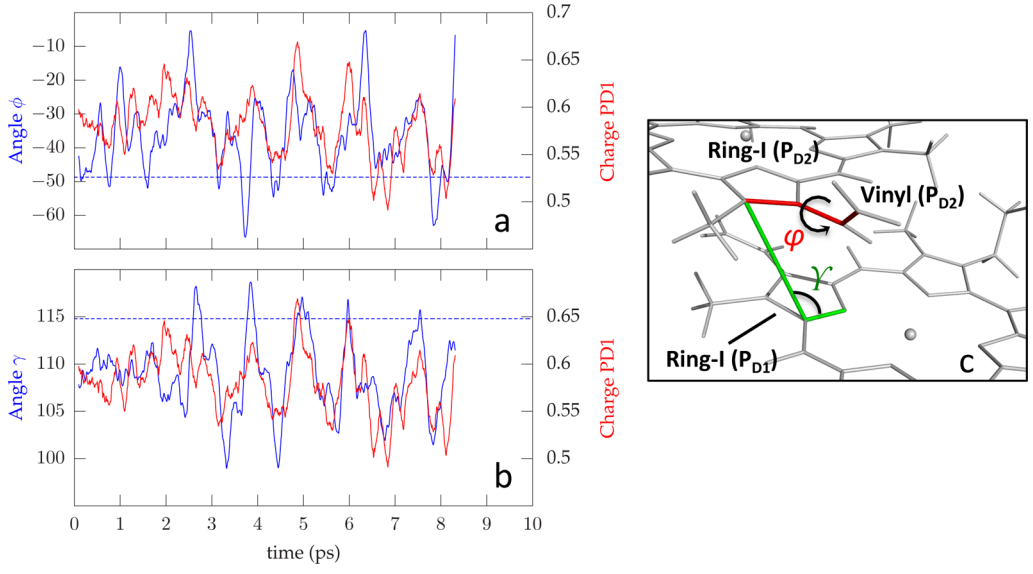

Figure 5. Slow molecular motions correlating with charge fluctuations in the $[P_{D1},P_{D2}]^{\bullet+}_{AIMD}$ system. (a) Time evolution of the partial charge present on on P_{D1} in the oxidized system (red line) and the dihedral angle ϕ of the vinyl group of P_{D2} (blue line). The value of the charge and the dihedral angle is smoothed averaging over 40 frame blocks. The value of the dihedral angle relative to the the X-ray positions is indicated as blue dashed line. (b) Time evolution of the angle γ (defined in panel c) is shown as blue line. The value of the angle γ relative to the the X-ray positions is indicated as blue dashed line. The same smoothing procedure was adopted as in panel a. (c) Definition of the angles ϕ and γ.

significantly involved into the effective normal modes of the P_{D2}, whereas no contribution of such moieties was found in P_{D1}.

In addition to the frequency analysis detailed above, we have systematically searched for time correlations between charge fluctuations and intra- and intermolecular geometrical descriptors, with the aim to monitor the contributions of the slowest motions, which cannot be properly described by a Fourier analysis of a picosecond trajectory. Among the others, we checked the possible correlations between the orientations

DOI: 10.1021/jacs.5b10523
J. Am. Chem. Soc. 2016, 138, 257−264

of the vinyl groups and the charge fluctuations. The vinyl group corresponds to the acetyl group of the bacteriochlorophyll-a special pair, whose orientation was suggested to effect the redox potential of the special pair. We found no correlation along the trajectory between the orientation of the vinyl group and the partial charge localized on the P_{D1} chlorophyll, whereas a poor correlation ($R^2 = 0.32$) was found between the dihedral angle ϕ of the vinyl group on the P_{D2} pigment and the charge fluctuation (see Figure 5a). A slightly higher correlation ($R^2 = 0.50$) was found between the charge fluctuations and the angle γ, describing the reciprocal orientation of the two rings I belonging to the P_{D1} and the P_{D2} (see Figure 5b,c). Additional analysis of the data using the Eureqa software[33] indicates that nonlinear functions of the two variables ϕ and γ lead to higher correlation, suggesting that they are important in the charge modulation. Our results indicate that charge fluctuations between the special pair chlorophylls of PSII are affected by both intra- and intermolecular motions at different time ranges.

DISCUSSION

Understanding of the determinants responsible for the charge separation occurring in the chlorophyll special pair of photosystem II is of central importance to obtain a clear and complete view of the enzyme function and, eventually, its photoprotective mechanism. Here, using both static and *ab initio* QM/MM molecular dynamics calculations, we addressed the issue of the influence of thermal fluctuations on the charge distribution over the oxidized chlorophylls special pair.

From static calculations carried out on the X-ray structure as well as the geometry optimized structure, we found a charge ratio of the two chlorophylls, $P_{D1}^{\bullet+}/P_{D2}^{\bullet+}$, close to 0.80/0.20, in agreement with previous theoretical[14,15] and experimental[12,34] studies. Nevertheless, to obtain a detailed picture of the events occurring at physiological temperature in the first picoseconds following the oxidation of the special pair, the effect of the thermal fluctuations on the charge distribution has to be taken into account.[4] Moreover, the thermal effects can strongly effect the short-range interactions that modulate the electronic coupling in such systems.[35] In this regard, from comparative studies with the purple bacterial P_L/P_M pair, it was suggested that the reciprocal orientation of ring I in the chlorophylls special pair in PSII may have a deep impact on the orbital overlap.[5] We therefore carried out MD simulations at a temperature of 298 K in a QM/MM framework considering the quantum center composed by the chlorophyll special pair rings and the two coordinated histidines in both neutral and oxidized state. In the neutral state, the average charge ratio $P_{D1}^{\bullet+}/P_{D2}^{\bullet+}$ was found to be equal to 0.54/0.46 with several charge inversions between the two pigments. To simulate the first picoseconds following the initial charge separation, we carried out a QM/MM simulation starting from one snapshot of the neutral system simulation removing an electron from the quantum center. Along the ∼8 ps of simulation, we found an average charge ratio $P_{D1}^{\bullet+}/P_{D2}^{\bullet+}$ equal to 0.59/0.41 with large charge fluctuations (from ∼0.8/0.2 to ∼0.4/0.6). From our analysis, we found that the main determinant for the different charge distribution in the X-ray structure compared with the QM/MM molecular dynamics resides in the relative orientation fo the two rings I in the chlorophylls P_{D1} and P_{D2}. Indeed, the value of the angle γ (defined in Figure 5c) as found in the X-ray structure is 114.8° (see dashed line in Figure 5b), which is considerably larger compared with the average value calculated along 8 ps of simulation ($\gamma = 108.9°$). Although additional determinants contribute to the modulation of the charge distribution over the two pigments, the relative orientation of the two rings I experienced along the dynamics strongly affects such modulation, increasing or decreasing the coupling between the two chlorophylls and the respective charge distribution.

The effect of the dynamics is therefore changing qualitatively the picture of the charge delocalization, which, at physiological temperature, is much less pronounced than previously though. Whereas the preferential localization of the cation is, as expected,[13,24] still the P_{D1} chlorophyll, occasional inversions of the charge distribution are always present even along short picosecond dynamics. This behavior can have a strong impact in photoprotection mechanisms of photosystem II. Indeed, the transient localization of the cation on P_{D2} may serve as an electron acceptor from the β-carotene/Cyt $b559$/ChlZ_{D2} side pathway,[5,17,18] playing a crucial role in the PSII cyclic electron transfer.[36] Another photoprotective mechanism fulfilled by the photosystem II supercomplex consists of non-photochemical chlorophyll fluorescence quenching. Two different hypotheses have been proposed about the location of the charge recombination at the basis of this mechanism. The quenching could either arise from a charge recombination between the $P680^+$ and the acceptor side of photosystem II or occur in the antenna system of PSII, this second proposal being the most widely accepted in the last years.[37] Although based on our calculations it is not possible give a definitive answer, the high degree of charge delocalization found in the present study discourages the hypothesis of a fast charge recombination between $P680^+$ and the acceptor side of PSII.

The calculations also revealed the role of the protein surroundings and of the dynamics on tuning of the asymmetric behavior of the charge. Albeit, based on static QM/MM calculations, the asymmetric charge distribution between the P_{D1} and the P_{D2} pigments was found to mainly be due to the electrostatic interaction with different protein residues, the dynamical charge fluctuations reported in this study clearly show a strong modulation by intra- and intermolecular conformational changes. In particular, combining the vibrational analysis of the special pair and the Fourier analysis of the charge displacement between P_{D1} and P_{D2}, we showed that specific frequencies in the charge oscillations can be associated with specific effective normal modes of the two pigments.

In a recent paper, Romero et al.[29] revealed the presence of coherence between excitons and charge-transfer states. They suggested that such coherence is maintained by vibrational modes. In this regard, our results identify the power spectrum of the charge oscillation between the chlorophills and may therefore help to rationalize which intramolecular motions mostly contribute to the observed coherence effects.

Apart from fast intramolecular nuclear motions, we also monitored slower intra- and intermolecular motions, although this analysis may suffer from the short sampling. Nevertheless, we were able to identify significant correlation between the charge fluctuations and the relative orientation of ring I in the two P_{D1} and P_{D2} chlorophylls. It was suggested that the different behavior between the chlorophylls pair of the bacterial reaction center and the special pair of the photosystem II may arise from the different overlay of the two ring I.[38] Indeed in the X-ray structure of PSII, the π-stacking interaction is disrupted by an in-plane tilt of the macrocycle that was proposed to be necessary to localize the hole state.[38] Our results corroborated this hypothesis finding in the relative

DOI: 10.1021/jacs.5b10523
J. Am. Chem. Soc. 2016, 138, 257−264

orientation between the two rings a determinant for the localization of the cationic state over a specific chlorophyll.

Different studies focused on the localization of the excited state over the six pigments of the reaction center, which was found to depend on the temperature. In particular, at 5 K, the excited state was suggested to be strongly localized on Chl_{D1}, while at 300 K, it turns out to be delocalized over the six pigments as assumed in the multimer model.[38] Although in our calculations we did not explicitly take into account excited states and the calculations are restricted to two chlorophylls, we can suggest that, as thermal fluctuations modulate the HOMO distribution over the neutral special pairs of chlorophylls, a similar mechanism may modulate the localization of the excited state. Overall, our results confirm the importance to take into account the conformations sampled by the pigments of PSII at physiological conditions and the subsequent effect on their coupling in order to accurately describe the charge separation and the excitation energy transfer mechanisms.[39]

In conclusion, finite temperature dynamics has an important effect on the charge distribution of the special pairs of chlorophylls in photosystem II. Charge is indeed much less localized than in the usual static picture, and the two chloropylls are strongly coupled, in line with the idea that collective motions are dominant, as was suggested for the primary charge separation.[40]

METHODS

Simulated System. The QM/MM model considered in the present study was built by extracting a region of about 40 000 atoms from a model of the dimeric PSII complex embedded in a membrane bilayer after performing a classical MD simulation with position restraints on the X-ray coordinates (PDB ID 3ARC[2]). The QM/MM model includes, as classical part, all of the amino acids of the D1, D2, and CP43 polypeptide chains, the neighboring cofactors, and the water molecules present in the structure (further details reported in ref 41). From this model, we have selected as quantum region the two chlorophyll rings, P_{D1} and P_{D2} (without their phytol side chains), and the side chains of the Mg-coordinated histidines, D1-His198 and D2-His197 (see also Figure 1). Both the histidines and the chlorophylls are saturated with capping hydrogen atoms on the carbon atoms linking the QM and the MM systems. In QM/MM and gas phase calculations, two different oxidation states of the quantum system were considered: the reduced state, $[P_{D1},P_{D2}]^{0}$ (neutral QM system with singlet multiplicity, treated with restricted Kohn−Sham DFT scheme), and the oxidized state, $[P_{D1},P_{D2}]^{\bullet+}$ (+1 charged QM system with doublet multiplicity, treated with unrestricted Kohn−Sham DFT scheme). For both QM/MM oxidation states, *ab initio* molecular dynamics, $[P_{D1},P_{D2}]^{0/\bullet+}_{AIMD}$, and QM/MM geometry optimization with a constraint to the MM part, $[P_{D1},P_{D2}]^{0/\bullet+}_{QM/MM}$, were carried out. To better understand the role of the geometry and the protein environment on the charge stabilization, we also considered analogous models as gas phase isolated systems: $[P_{D1},P_{D2}]^{0/\bullet+}_{GP-X\text{-}ray}$ (with heavy atoms constrained to X-ray coordinates),[2] $[P_{D1},P_{D2}]^{0/\bullet+}_{GP}$ (fully relaxed in gas phase), and $[P_{D1},P_{D2}]^{0/\bullet+}_{GP-from\text{-}QM/MM}$ (same geometry as $[P_{D1},P_{D2}]^{0/\bullet+}_{QM/MM}$ but without the protein field).

Computational Details. QM/MM calculations were performed using the CP2K package.[42,43] General AMBER force field (GAFF)[44] was used for the classical description of the cofactors embedded in the QM/MM region, whereas the standard protein residues were described by AMBER99SB force field,[45] consistently with our previous studies.[31,32,41] For the description of the electronic structure of the quantum region, we used the Kohn−Sham DFT scheme using the functional Perdew−Burke−Ernzerhof.[46] Goedecker−Teter−Hutter pseudopotentials[47,48] were used for all the atoms in the QM region. The Gaussian/plane-wave scheme[42] implemented in the CP2K package was used in all the QM/MM calculations with DZVP-MOLOPT-SR-GTH Gaussian basis set optimized for molecular systems.[49] A cut off of 320 Ry was set for the plane-wave basis set.

The QM/MM Born−Oppenheimer *ab initio* molecular dynamics of the reduced and oxidized systems, $[P_{D1},P_{D2}]^{0/\bullet+}_{AIMD}$, were performed with a time step of 0.5 fs in NVT ensemble with the Nosé−Hoover thermostat[50−52] (T = 298 K). During the dynamics, the positions of all α-carbon atoms as well as the Mn_4CaO_5 cluster were kept fixed. The two QM/MM *ab initio* molecular dynamics were carried out for a total computed time of 3 ps of thermalization and 12 ps dynamics for $[P_{D1},P_{D2}]^{0}_{AIMD}$ and 3 ps of thermalization and 8 ps dynamics for the most expensive unrestricted $[P_{D1},P_{D2}]^{\bullet+}_{AIMD}$ system.

To follow the electronic structure properties of the special pair along dynamics, snapshots were extracted from both the reduced and the oxidized AIMD every 50 fs. The localization of molecular orbitals on the two chlorophylls was followed by projecting the electronic density of states on the P_{D1} and P_{D2} atoms. Similarly, to follow the charge localization in the oxidized dynamics, we sum the total charges of the atoms of the two chlorophylls as derived by population analysis. In the reduced dynamics, $[P_{D1},P_{D2}]^{0}_{AIMD}$, we have also monitored the asymmetry in the propensity for oxidation by analyzing the electronic structure upon removal of one electron for each of the frames extracted.

Vibrational Analysis. The characteristic frequencies of the charge fluctuations of the oxidized special pair were obtained in the range of 300−1800 cm^{-1} by the Fourier analysis of the charge difference between P_{D1} and P_{D2}, calculated by summing the Mulliken charges on each chlorophyll.

In order to understand the dependence of the charge on the molecular motions, the vibrational analysis of the P_{D1} and P_{D2} atomic trajectories from the $[P_{D1},P_{D2}]^{\bullet+}_{AIMD}$ was performed and the frequency couplings were evaluated. The total vibrational density of states (VDOS) has been computed through the Fourier transform of the atomic velocity−velocity autocorrelation function. Collective molecular motions associated with the peaks observed in the VDOS are obtained by effective normal-mode analysis, that is, the finite-temperature analogous to zero-temperature normal-mode analysis. The vibrational analysis of the single chlorophylls were obtained by extracting the atomic coordinates and velocities of the two chlorophylls singularly. Effective normal mode decomposition was carried out by maximally localizing the vibrational density of states of each normal mode, using the techniques described in ref 53, already successfully applied to characterize biomolecular vibrations at finite temperature in solution.[54,55] The vibrational spectrum of each normal mode was compared with the charge DOS spectrum, calculating the overlap with selected peaks.

To visualize which moieties of the chlorophylls are involved in such charge-modulating modes, we evaluated the atomic contribution to each of the above-selected effective normal modes, calculating the square of the corresponding displacement vector times the atomic mass. The influence of each atom on the charge fluctuations is obtained by summing the atomic contribution of every effective normal mode weighted according to its overlap factor. The data are therefore visualized on the P_{D1} and P_{D2} molecular structures using a color scale.

ASSOCIATED CONTENT

Supporting Information

The Supporting Information is available free of charge on the ACS Publications website at DOI: 10.1021/jacs.5b10523.

Time evolution of partial charges present on P_{D1} and P_{D2} for the neutral and oxidized systems (PDF)

AUTHOR INFORMATION

Corresponding Author

*l.guidoni@univaq.it

Notes

The authors declare no competing financial interest.

DOI: 10.1021/jacs.5b10523
J. Am. Chem. Soc. 2016, 138, 257−264

■ ACKNOWLEDGMENTS

The authors acknowledge funds provided by the European Research Council project n. 240624 within the VII Framework Program of the European Union. We also thanks Massimo Trotta for useful discussions. The computational resources were supplied by PRACE infrastructure and by the Caliban-HPC center at the University of L'Aquila.

■ REFERENCES

(1) Barber, J. *Chem. Soc. Rev.* **2009**, *38*, 185−196.
(2) Umena, Y.; Kawakami, K.; Shen, J.-R.; Kamiya, N. *Nature* **2011**, *473*, 55−60.
(3) Croce, R.; van Amerongen, H. *J. Photochem. Photobiol., B* **2011**, *104*, 142−153.
(4) Zhang, L.; Silva, D.-A.; Zhang, H.; Yue, A.; Yan, Y.; Huang, X. *Nat. Commun.* **2014**, *5*, 4170.
(5) Cardona, T.; Sedoud, A.; Cox, N.; Rutherford, A. W. *Biochim. Biophys. Acta, Bioenerg.* **2012**, *1817*, 26−43.
(6) Shkuropatov, A. Y.; Khatypov, R. A.; Volshchukova, T. S.; Shkuropatova, V. A.; Owens, T. G.; Shuvalov, V. A. *FEBS Lett.* **1997**, *420*, 171−174.
(7) Shkuropatov, A. Y.; Khatypov, R. A.; Shkuropatova, V. A.; Zvereva, M. G.; Owens, T. G.; Shuvalov, V. A. *FEBS Lett.* **1999**, *450*, 163−167.
(8) Stewart, D. H.; Brudvig, G. W. *Biochim. Biophys. Acta, Bioenerg.* **1998**, *1367*, 63−87.
(9) Wang, J.; Gosztola, D.; Ruffle, S. V.; Hemann, C.; Seibert, M.; Wasielewski, M. R.; Hille, R.; Gustafson, T. L.; Sayre, R. T. *Proc. Natl. Acad. Sci. U. S. A.* **2002**, *99*, 4091−4096.
(10) Tracewell, C. A.; Brudvig, G. W. *Biochemistry* **2008**, *47*, 11559−11572.
(11) Thompson, L. K.; Brudvig, G. W. *Biochemistry* **1988**, *27*, 6653−6658.
(12) Diner, B. A.; Schlodder, E.; Nixon, P. J.; Coleman, W. J.; Rappaport, F.; Lavergne, J.; Vermaas, W. F.; Chisholm, D. A. *Biochemistry* **2001**, *40*, 9265−9281.
(13) Groot, M. L.; Pawlowicz, N. P.; van Wilderen, L.; Breton, J.; van Stokkum, I. H. M.; van Grondelle, R. *Proc. Natl. Acad. Sci. U. S. A.* **2005**, *102*, 13087−13092.
(14) Saito, K.; Ishida, T.; Sugiura, M.; Kawakami, K.; Umena, Y.; Kamiya, N.; Shen, J.; Ishikita, H. *J. Am. Chem. Soc.* **2011**, *133*, 14379−14388.
(15) Saito, K.; Umena, Y.; Kawakami, K.; Shen, J. R.; Kamiya, N.; Ishikita, H. *Biochemistry* **2012**, *51*, 4290−4299.
(16) Romero, E.; van Stokkum, I. H. M.; Novoderezhkin, V. I.; Dekker, J. P.; van Grondelle, R. *Biochemistry* **2010**, *49*, 4300−4307.
(17) Tracewell, C. A.; Vrettos, J. S.; Bautista, J. A.; Frank, H. A.; Brudvig, G. W. *Arch. Biochem. Biophys.* **2001**, *385*, 61−69.
(18) Faller, P.; Fufezan, C.; Rutherford, A. W. *Adv. Photosynth. Respir.* **2005**, *22*, 347−365.
(19) Zouni, A.; Witt, H. T.; Kern, J.; Fromme, P.; Krauss, N.; Saenger, W.; Orth, P. *Nature* **2001**, *409*, 739−743.
(20) Loll, B.; Kern, J.; Saenger, W.; Zouni, A.; Biesiadka, J. *Nature* **2005**, *438*, 1040−1044.
(21) Guskov, A.; Kern, J.; Gabdulkhakov, A.; Broser, M.; Zouni, A.; Saenger, W. *Nat. Struct. Mol. Biol.* **2009**, *16*, 334−342.
(22) Suga, M.; Akita, F.; Hirata, K.; Ueno, G.; Murakami, H.; Nakajima, Y.; Shimizu, T.; Yamashita, K.; Yamamoto, M.; Ago, H.; Shen, J. R. *Nature* **2015**, *517*, 99−103.
(23) Noguchi, T.; Tomo, T.; Inoue, Y. *Biochemistry* **1998**, *37*, 13614−13625.
(24) Holzwarth, A. R.; Muller, M. G.; Reus, M.; Nowaczyk, M.; Sander, J.; Rogner, M. *Proc. Natl. Acad. Sci. U. S. A.* **2006**, *103*, 6895−6900.
(25) Okubo, T.; Tomo, T.; Sugiura, M.; Noguchi, T. *Biochemistry* **2007**, *46*, 4390−4397.
(26) Novoderezhkin, V. I.; Romero, E.; Dekker, J. P.; van Grondelle, R. *ChemPhysChem* **2011**, *12*, 681−688.
(27) Ishikita, H.; Saenger, W.; Biesiadka, J.; Loll, B.; Knapp, E.-W. *Proc. Natl. Acad. Sci. U. S. A.* **2006**, *103*, 9855−9860.
(28) Raszewski, G.; Renger, T. *J. Am. Chem. Soc.* **2008**, *130*, 4431−4446.
(29) Romero, E.; Augulis, R.; Novoderezhkin, V. I.; Ferretti, M.; Thieme, J.; Zigmantas, D.; van Grondelle, R. *Nat. Phys.* **2014**, *10*, 676−682.
(30) Fuller, F. D.; Pan, J.; Gelzinis, A.; Butkus, V.; Senlik, S. S.; Wilcox, D. E.; Yocum, C. F.; Valkunas, L.; Abramavicius, D.; Ogilvie, J. P. *Nat. Chem.* **2014**, *6*, 706−711.
(31) Bovi, D.; Narzi, D.; Guidoni, L. *Angew. Chem., Int. Ed.* **2013**, *52*, 11744−11749.
(32) Narzi, D.; Bovi, D.; Guidoni, L. *Proc. Natl. Acad. Sci. U. S. A.* **2014**, *111*, 8723−8728.
(33) Schmidt, M.; Lipson, H. *Science* **2009**, *324*, 81−85.
(34) Rigby, S. E. J.; Nugent, J. H. A.; O'Malley, P. J. *Biochemistry* **1994**, *33*, 10043−10050.
(35) Madjet, M. E. A.; Muh, F.; Renger, T. *J. Phys. Chem. B* **2009**, *113*, 12603−12614.
(36) Derks, A.; Schaven, K.; Bruce, D. *Biochim. Biophys. Acta, Bioenerg.* **2015**, *1847*, 468−485.
(37) Ruban, A. V.; Johnson, M. P.; Duffy, C. D. P. *Biochim. Biophys. Acta, Bioenerg.* **2012**, *1817*, 167−181.
(38) Raszewski, G.; Diner, B. A.; Schlodder, E.; Renger, T. *Biophys. J.* **2008**, *95*, 105−119.
(39) Renger, G.; Renger, T. *Photosynth. Res.* **2008**, *98*, 53−80.
(40) Peterman, E. J. G.; van Amerongen, H.; van Grondelle, R.; Dekker, J. P. *Proc. Natl. Acad. Sci. U. S. A.* **1998**, *95*, 6128−6133.
(41) Bovi, D.; Narzi, D.; Guidoni, L. *New J. Phys.* **2014**, *16*, 015020.
(42) VandeVondele, J.; Krack, M.; Mohamed, F.; Parrinello, M.; Chassaing, T.; Hutter, J. *Comput. Phys. Commun.* **2005**, *167*, 103−128.
(43) Laino, T.; Mohamed, F.; Laio, A.; Parrinello, M. *J. Chem. Theory Comput.* **2005**, *1*, 1176−1184.
(44) Wang, J.; Wolf, R. M.; Caldwell, J. W.; Kollman, P. A.; Case, D. A. *J. Comput. Chem.* **2004**, *25*, 1157−1174.
(45) Hornak, V.; Abel, R.; Okur, A.; Strockbine, B.; Roitberg, A.; Simmerling, C. *Proteins: Struct., Funct., Genet.* **2006**, *65*, 712−725.
(46) Perdew, J. P.; Burke, K.; Ernzerhof, M. *Phys. Rev. Lett.* **1996**, *77*, 3865−3868.
(47) Goedecker, S.; Teter, M.; Hutter, J. *Phys. Rev. B: Condens. Matter Mater. Phys.* **1996**, *54*, 1703−1710.
(48) Hartwigsen, C.; Goedecker, S.; Hutter, J. *Phys. Rev. B: Condens. Matter Mater. Phys.* **1998**, *58*, 3641−3662.
(49) VandeVondele, J.; Hutter, J. *J. Chem. Phys.* **2007**, *127*, 114105.
(50) Hoover, W. G. *Phys. Rev. A: At., Mol., Opt. Phys.* **1985**, *31*, 1695−1697.
(51) Nosé, S. *J. Chem. Phys.* **1984**, *81*, 511−519.
(52) Nosé, S. *Mol. Phys.* **1984**, *52*, 255−268.
(53) Gaigeot, M. P.; Martinez, M.; Vuilleumier, R. *Mol. Phys.* **2007**, *105*, 2857−2878.
(54) Bovi, D.; Mezzetti, A.; Vuilleumier, R.; Gaigeot, M. P.; Chazallon, B.; Spezia, R.; Guidoni, L. *Phys. Chem. Chem. Phys.* **2011**, *13*, 20954−20964.
(55) Zhang, C.; Naziga, E. B.; Guidoni, L. *J. Phys. Chem. B* **2014**, *118*, 11487−11495.

DOI: 10.1021/jacs.5b10523
J. Am. Chem. Soc. 2016, 138, 257−264